

A&A manuscript no.
(will be inserted by hand later)

Your thesaurus codes are:
08 (02.13.5; 09.01.1; 09.03.1; 09.13.2; 09.09.1 CrA, Cha I)

Molecular line study of evolution in protostellar cloud cores

S. Kontinen¹, J. Harju¹, A. Heikkilä¹ and L.K. Haikala^{1,2}

¹ Observatory, P.O. Box 14, FIN-000 14 University of Helsinki, Finland

² Swedish-ESO Submillimetre Telescope, European Southern Observatory, Casilla 19001, Santiago, Chile

Received 11.04.2000; accepted 14.07.2000

Abstract. Two dense dark cloud cores representing different stages of dynamical evolution were observed in a number of molecular spectral lines. One of the cores, Cha-MMS1 in the Chamaeleon cloud I contains a Class 0 protostar, whereas the other, CrA C in the R Coronae Australis cloud, is pre-stellar. The molecules selected for this study are supposed to show significant abundance variations in the course of the chemical evolution.

We find that the cores have very different chemical compositions. Cha-MMS1 exhibits characteristics of so-called ‘early-type’ chemistry with high abundances of carbon-chain molecules such as HC₃N, CH₃CCH and c-C₃H₂. However, it also has a large N₂H⁺ abundance, which is expected only to build up at later stages. In contrast, none of the carbon-chain molecules were detected in CrA C. On the other hand, CrA C has a higher SO abundance than Cha-MMS1, which according to chemistry models implies that it is chemically ‘older’ than Cha-MMS1. The most striking difference between the two cores is seen in the HC₃N/SO abundance ratio, which is at least three orders of magnitude higher in Cha-MMS1 than in CrA C. This result is somewhat surprising since starless cores are usually thought to be chemically younger than star-forming cores.

Because of the high N₂H⁺ abundance, we suggest that Cha-MMS1 represents the ‘late-time cyanopolyne peak’ that is predicted to occur when heavy molecules start to freeze onto grain surfaces (Ruffle et al. 1997). This would also be a more natural explanation for the carbon-chain molecules than the ‘early-time’ picture in view of the fact that the core is presently collapsing to form a star. The abundances observed in CrA C can be explained either by pure gas-phase models at late stages of evolution, or by the ‘SO peak’ which follows the second cyanopolyne peak (Ruffle et al. 1999). Thus, the dynamical evolution in CrA C seems to have been very slow compared with that of Cha-MMS1, and we discuss possible reasons for this.

We detected two SO emission maxima around Cha-MMS1, which lie symmetrically on both sides of the core,

approximately on the line connecting the centre of Cha-MMS1 and the position of Herbig-Haro object HH49/50. These SO peaks may signify the lobes of a bipolar outflow, and the observation supports the suggestion by Reipurth et al. 1996 that Cha-MMS1 is the central source of HH49/50.

Key words: molecular processes – ISM: abundances, clouds, molecules – individual: CrA C, Cha-MMS1

1. Introduction

To understand the first steps of the star-formation process, we must be able to follow the evolution of molecular cloud cores. One approach is to conduct spectral-line observations of molecular species whose abundances vary significantly with time. Conversely, combining such observations with other types of diagnostics of cloud evolution, the chemical models may be tested.

Examples of species that are believed to be useful for the aforementioned purposes are complex hydrocarbons and cyanopolyynes¹. Their abundances are expected to peak at early stages of the evolution of dark clouds (e.g. Herbst & Leung 1989). This is because their production requires a high abundance of free neutral carbon (C I); a condition that is satisfied at early times in the chemical evolution, whereas at later stages practically all free carbon has been exhausted in the production of CO. In contrast, molecules such as NH₃ and SO increase in abundance with time, because their formation involves relatively slow neutral-neutral reactions (Suzuki et al. 1992; Hirahara et al. 1995; Nilsson et al. 2000), or because they (e.g. SO) are destroyed by C I or C⁺.

The validity of these model predictions have, to date, been tested in a rather limited sample of dark cloud cores. Most observations have been confined to the Taurus Molecular Cloud 1 (TMC-1), L134A, and to a number of “Myers’ cores” (Pratap et al. 1997; Swade 1989;

¹ Molecules with the generic form HC_(2n+1)N where n = 1, 2, ...

Myers & Benson 1983, Benson et al. 1998; for a review see van Dishoeck & Blake 1998). However, for current chemistry models to be rigorously tested, the cloud sample needs to be more representative of the ISM. In the present paper we extend the sample of well-studied objects by two potentially very young molecular cloud cores.

The first core selected for this study is located in the region of the reflection nebula Cederblad 110 in the Chamaeleon dark cloud I. Reipurth et al. 1996 detected a strong 1.3mm dust continuum source towards this core, and designated it as Cha-MMS1. The core belongs to an extensive, northeast–southwest directed filament of dense gas near the centre of this cloud (Mattila et al. 1989). The second core, CrA C (Harju et al. 1993) is located in the southeastern ‘tail’ of the R Coronae Australis molecular cloud. The distances to the Chamaeleon I and the R Coronae Australis clouds are 150 and 170 pc, respectively (Knude & Høg 1998). The smallest diameters of the C¹⁸O cores are 0.11 and 0.05 pc for CrA C and Cha-MMS1, respectively. The C¹⁸O column densities towards both cores are similar: $N(\text{C}^{18}\text{O}) \sim 2 \cdot 10^{15} \text{ cm}^{-2}$, which corresponds to a molecular hydrogen column density of $N(\text{H}_2) \sim 10^{22} \text{ cm}^{-2}$ (Harju et al. 1993; Mattila et al. 1989). The average H₂ densities derived from these numbers assuming prolate geometries are $\sim 3 \cdot 10^4$ and $\sim 7 \cdot 10^4 \text{ cm}^{-3}$ for CrA C and Cha-MMS1, respectively. The kinetic temperature in CrA C is 10 K or less (Harju et al. 1993), whereas in Cha-MMS1 the gas kinetic temperature as derived from ammonia observations is slightly elevated with respect to the typical dark cloud value, being ~ 14 K (Toth et al. 2000, in preparation).

Even though both cores are supposed to be young, they represent different stages of cloud evolution. Cha-MMS1 probably contains a Class 0 protostar (Reipurth et al. 1996), which has been recently identified with a far-infrared source, designated Ced110 IRS 10, by Lehtinen et al. 2000. The core lies next to a small group of newly-born stars, the closest being Ced 110 IRS 4 (Prusti et al. 1991) and the newly detected IRS 11 (Lehtinen et al. 2000), which belong to the infrared source Class I. The core is associated with a compact, north-south oriented molecular outflow (Mattila et al. 1989; Prusti et al. 1991; Lehtinen et al. 2000). Reipurth et al. 1996 suggested that Cha-MMS1 contains the driving source of the outflow and the Herbig-Haro objects HH 49/50 located some 10' south of the core.

CrA C shows no sign of star formation activity. The core appears to be surrounded by an extensive halo: it is located near the centre of a neutral atomic hydrogen ring with a diameter of 40' (Llewellyn et al. 1981) which may represent the outer boundary of a massive HI to H₂ conversion region. Observations of continuum emission at 100 μm and 200 μm wavelengths with the ISOPHOT instrument on the Infrared Space Observatory (ISO) reveal a 200 μm excess coinciding with the centre of CrA C

(Heikkilä et al. 2000, in preparation), suggesting that a very cold clump is located inside this core.

Based on these facts, one could expect CrA C to exhibit the characteristics of ‘early time’ chemistry, e.g. high abundances of unsaturated carbon compounds, whereas Cha-MMS1 could be thought to have reached a more evolved stage. In order to test these ideas, we have estimated for these dense cores the column densities of several molecules which show significant time dependence in chemistry models.

The selected molecules are discussed in the next Section. In Sect. 3 we describe the observational procedure. In Sect. 4 the results from the observations are presented and these are further discussed in Sect. 5. Finally, in Sect. 6 we summarize our conclusions.

2. Observed molecules

We discuss here the spectroscopic and chemical properties of the molecules included in this study. Table 1 lists their chemical formulae, structure types (hfs means that the lines have hyperfine structure; o/p and *A/E* that the molecule has ortho and para or *A*-symmetry and *E*-symmetry forms, respectively), permanent electric dipole moments (μ_{electric}) along the relevant molecular axes, and rotational constants (*A*, *B* and *C*). The data were extracted mainly from the JPL catalogue² (Poynter & Pickett 1985); exceptions are the CH₃OH data (Sastry et al. 1981; Anderson et al. 1990) and the value for the dipole moment of CCS (Murukami 1990).

2.1. Spectroscopic properties

Carbon monosulphide, **CS**, is a linear molecule with a simple rotational spectrum; the states are denoted by the total angular momentum quantum number *J*. The simplicity of the spectrum is due to the facts that in the electronic ground state, the electrons in the CS molecule have paired spins and possess no orbital angular momentum. Hence, the ground state is denoted ¹Σ. In addition, the C and S nuclei have no spin.

The dicarbon sulphide radical, **CCS**, and the sulphur monoxide radical, **SO**, have more complicated spectra than CS. The electrons in the electronic ground states of CCS and SO have no net orbital angular momentum, but the total spin is non-zero due to two electrons having unpaired spins. Thus, the spin quantum number is *S* = 1 and the electronic ground state is denoted ³Σ (e.g. Gordy & Cook 1970, Sect. 4.2). The electron spin is coupled to the weak magnetic field arising from the rotation of the molecule. Since *S*=1, for each molecular

² An updated version is available on the WWW at <http://spec.jpl.nasa.gov>.

rotational level with the rotational angular momentum quantum number $N > 0$, the total angular momentum quantum number, J , has three possible values: $J = N - 1$, $J = N$ or $J = N + 1$. Consequently, the rotational levels $N > 0$ are split into triplets, whereas for $N=0$ only one state ($J_N = 1_0$) exists (e.g. Yamamoto et al. 1990).

Hydrogen isocyanide, **HNC**, is a linear molecule. The nitrogen nucleus has a non-zero spin, and therefore possesses an electric quadrupole moment. This interacts with the electric field gradient of the molecule, which depends on the rotation. Consequently, the nuclear spin ($I = 1$) is coupled to the molecular rotational angular momentum, J , to yield the total angular momentum, F (Gordy & Cook 1970, Sect. 9.4). The resulting hyperfine splitting of the rotational lines of HNC is smaller than for its isomer HCN. For example, for the lowest rotational transition ($J = 1 \rightarrow 0$) the $F = 1 \rightarrow 1$ and $F = 0 \rightarrow 1$ components are separated from the main component $F = 2 \rightarrow 1$ by -0.27 and $+0.41 \text{ km s}^{-1}$ respectively (Frerking et al. 1979). Hence, the hyperfine structure is usually not resolved in observations due to Doppler broadening in the source and the insufficient spectral resolution of the spectrometers available.

Cyanoacetylene, **HC₃N**, is also a linear molecule. Due to its high moment of inertia, it has a small rotational constant (B) and its rotational transitions $J \rightarrow J - 1$ lie relatively closely in frequency. Many of these lines are located in the commonly observed frequency bands, and it is often used in multi-transition studies. Like HNC, it has hyperfine structure due to the nuclear spin of nitrogen. For higher J -values, however, the relative energy differences between different F -levels are very small, and so no hyperfine structure is seen in the spectra observed here.

Methyl acetylene, **CH₃CCH**, is a low dipole moment, symmetric top molecule. Its energy levels are described by two quantum numbers J and K . The former represents the total angular momentum and the latter is the projection of J on the symmetry axis of the molecule. The lowest energy state in each K -ladder is $J=K$. CH₃CCH exists in two chemically different forms, the so called A and E symmetry species, depending on the relative orientations of the spins of the three hydrogen nuclei in the CH₃ group. For the A -symmetry species, the K quantum numbers are multiples of 3 (i.e. $K = 3n$; $n=0,1,2,\dots$), while the E -symmetry species has $K = 3n + 1$ and $3n + 2$; $n=0,1,2,\dots$. The ground-state energies for A and E CH₃CCH differ by 8.02K, E lying higher in energy. There are no allowed electric dipole transitions between two states belonging to different K -ladders. Consequently, the relative populations of two K -ladders are determined by collisional transitions and therefore depend on the kinetic temperature. In fact, the so-called ‘rotational temperature’, which can be determined from

a single observation of a $J \rightarrow J - 1, K$ -multiplet (the lines lie closely in frequency), is considered to be a good approximation of the kinetic temperature (e.g. Bergin et al. 1994).

Cyclo-propenylidene, **c-C₃H₂**, is one of the few cyclic molecules detected in interstellar space. It is a slightly asymmetric, almost oblate top. C₃H₂ has *ortho*- and *para*-states originating from the two possible relative orientations of the spins of the two hydrogen nuclei (having $I = \frac{1}{2}$ each). In the *ortho*-state the spins are parallel ($I = 1$), whereas in the *para*-state the spins are anti-parallel ($I = 0$). Since the *ortho*- and *para*-forms cannot be interchanged in electric dipole transitions or easily in chemical reactions, they can be seen as two different chemical compounds. The ground-state of the *ortho*-form ($J_{K_a, K_c} = 1_{0,1}$) lies 2.35K higher than that of the *para*-form ($J_{K_a, K_c} = 0_{0,0}$). The electric dipole transitions of c-C₃H₂ are of *b*-type. This means that the quantum numbers describing the projection of J on the molecular *a*-axes and *c*-axes, K_a and K_c , change according to the rule $\Delta K_a = \pm 1$, $\Delta K_c = \pm 1$ (see Vrtilik et al. 1987).

Diazenylium, **N₂H⁺**, is a linear molecular ion. Its rotational transitions have hyperfine structure due to the coupling of the spins of the two nitrogen nuclei (I_1, I_2) to the rotational angular momentum (J). The energy levels are labelled using the quantum numbers J , F_1 and F , where $F_1 = J + I_1$ and $F = F_1 + I_2$ (e.g. Caselli et al. 1995; Gordy & Cook 1970, Sect. 9.5). The $J = 1 \rightarrow 0$ transition observed here has seven well resolved hyperfine components.

Methanol, **CH₃OH**, is a slightly asymmetric top (e.g. Townes & Schawlow 1975, chapters 4 & 12). It has a rather complicated rotational spectrum, since it exhibits so called hindered internal rotation: the hydroxyl (OH) group can rotate with respect to the methyl (CH₃) group. This gives rise to two different forms of CH₃OH between which both radiative and collisional transitions are forbidden: the A -symmetry and E -symmetry forms. Chemical reactions that might convert A to E or vice versa are believed to occur only on very long time scales. Therefore the two forms of CH₃OH can be treated as chemically distinct species. The ground-state of the E -symmetry form ($J_k = 1_{-1} E$) lies 6.95K higher than that of the A -symmetry form ($J_k = 0_0 A^+$). The relevant quantum numbers describing the rotational spectrum are J and k , with $k = K_a - K_c$. The electric dipole transitions observed here are of *a*-type, i.e. they obey the selection rule $\Delta k = 0$. Like other symmetric or slightly asymmetric tops, CH₃OH may provide useful information about the gas temperature.

2.2. Chemistry

The buildup of cyanopolyynes proceeds mainly via reactions between complex hydrocarbon ions and nitrogen atoms (Herbst & Leung 1989). HC_3N is the simplest cyanopolyne, and its abundance correlates well with heavier cyanopolyynes (e.g. Federman et al. 1990). Due to its large dipole moment, as well as being chemically an early-time species, HC_3N should be a useful probe of the conditions in pre-stellar cloud cores.

The main reactions leading to HC_3N and CH_3CCH involve either the C_3H_2^+ or C_3H_3^+ ions (Huntress & Mitchell 1979). The neutral reactions involving C_2H_2 and CCH suggested recently by Turner et al. 1998 and Turner et al. 1999 do not change this fact, since these species are also derivatives of the aforementioned molecular ions. Therefore, HC_3N and CH_3CCH abundances are expected to be well correlated.

Reactions of nitrogen-bearing ions, such as HCNH^+ , with neutral hydrocarbons may also contribute to the production of cyanopolyynes (Herbst & Leung 1989). Since HCNH^+ is the precursor ion of HCN and HNC (Herbst 1978), a correlation between these isomeric molecules and cyanopolyynes is possible. In this paper, we shall not address the as yet unresolved problem of the variation of the HNC/HCN abundance ratio from source to source (for a recent overview see e.g. Talbi & Herbst 1998). We instead used HNC merely to survey the extension of the core CrA C, where HC_3N was not detected. This should be as abundant as HCN but easier to detect due to the smaller hyperfine splitting,

In their survey towards dense cores of dark clouds, Suzuki et al. 1992 found a strong correlation between the CCS and HC_3N column densities, and, using data from Cox et al. 1989, a weaker correlation between CCS and C_3H_2 . They explained these correlations by the production of CCS in reactions between hydrocarbons and S^+ , which should be abundant in regions where also carbon-chain molecules are formed (Prasad & Huntress 1982). The formation of CS also involves S^+ and occurs in the very early stages of chemical evolution. Thereafter, CS is mainly recycled via the thioformyl ion, HCS^+ , and its abundance is considered to be rather constant in time (Nejad & Wagenblast 1999).

The correlation between HC_3N and CCS is due to fact that C_3H dominates the production of both molecules. HC_3N is related to C_3H_2 via the neutral-neutral reaction $\text{C}_3\text{H}_2 + \text{N} \rightarrow \text{HC}_3\text{N} + \text{H}$ (Herbst & Leung 1989; Nejad & Wagenblast 1999). On the other hand, complex carbon chain molecules and CCS show no correlation with ammonia, NH_3 (e.g. Little et al. 1979; Suzuki et al. 1992). This can be explained by the fact

that the production of NH_3 involves molecular nitrogen, N_2 , which is formed in neutral-neutral reactions and becomes abundant in the later stages of cloud evolution when carbon chain molecules have already been lost in reactions with ions such as He^+ , H^+ and H_3^+ (Suzuki et al. 1992). N_2H^+ is also formed from N_2 by $\text{N}_2 + \text{H}_3^+ \rightarrow \text{N}_2\text{H}^+ + \text{H}_2$ and its abundance has been found to follow closely that of NH_3 (Hirahara et al. 1995; Nejad & Wagenblast 1999). Therefore, if the CCS/NH_3 abundance ratio can be used as an age indicator as suggested by Suzuki et al. 1992, the same should be true for $\text{CCS}/\text{N}_2\text{H}^+$. The depletion of CO onto grain surfaces further increases the N_2H^+ abundance by making H_3^+ available for non-carbon bearing species to react with (Nejad & Wagenblast 1999).

SO is destroyed by neutral carbon and, like N_2H^+ , it is formed in neutral-neutral reactions and benefits from the freezing-out of CO . Its abundance therefore increases slowly and probably remains low as long as the gas is rich in neutral atomic carbon. The SO abundance first increases when carbon is consumed in the production of CO , i.e. at late stages in the chemical evolution (Bergin & Langer 1997; Nejad & Wagenblast 1999). The late peaking of SO and the stability of CS (until it too is frozen out) has led to the suggestion that the SO/CS abundance could be used as a chemical clock (Ruffle et al. 1999). Nilsson et al. 2000 came to the same conclusion on the basis of pure gas phase chemistry models. However, the SO/CS ratio is also sensitive to the gas-phase O/C ratio. Thus, when observing the SO/CS ratio in two individual clouds, it is not easy to disentangle the effects of time evolution from those of the O/C ratio.

The precursor ion of CH_3OH , CH_3OH_2^+ , is formed from the radiative association reaction between CH_3^+ and H_2O (e.g. Herbst & Leung 1989). The close relation to CH_3^+ makes CH_3OH an early-time molecule, as long as gas phase reactions are considered. The large abundances of CH_3OH in high-mass star-forming cores has been explained by evaporation from grain surfaces due to shock heating (e.g. Menten et al. 1988).

3. Observations

The observations were made in February 1998 at the Swedish-ESO Submillimetre Telescope (SEST) on La Silla in Chile. The 100 and 150 GHz SIS receivers were used simultaneously. These were connected to a 2000 channel acousto-optical spectrometer (AOS), which was split in two bands of 43 MHz each. The resulting channel-separations are 0.13 km s^{-1} (at 100 GHz) and 0.09 km s^{-1} (at 150 GHz), respectively. Calibration was achieved by the chopper-wheel method. The pointing and focus of the telescope were checked at 3-4 hours intervals against the

SiO($v = 1, J = 2 \rightarrow 1$) maser line towards AH Sco, U Men and R Dor. The pointing accuracy was typically $3''$ (rms) in each coordinate.

Most of the lines were observed in the frequency switching mode with a frequency throw of 6 MHz. Position switching was used for CH₃CCH and N₂H⁺ since the spectrometer band covers several of their lines.

The observations were started by mapping both sources in the HC₃N($J = 10 \rightarrow 9$) and SO($J_N = 4_3 \rightarrow 3_2$) transitions simultaneously in the frequency switching mode. HC₃N was not detected in CrA C, and therefore the map was repeated in the transition pair HNC($J = 1 \rightarrow 0$) & SO($J_N = 4_3 \rightarrow 3_2$). The rest of the observations were single position pointings towards the SO (in CrA C) or HC₃N (in Cha-MMS1) line emission peaks in these maps. Table 2 lists the (0, 0) positions used in the mapping observations and the peak positions, towards which the single pointing observations were made in each core.

In Table 3 we give a summary of the observed lines and some telescope characteristics at the corresponding frequencies. The columns of this Table are: (1) the rest-frequency; (2) the molecule; (3) the transition; (4) the line strength of the transition (S_{ul}); (5) the energy of the upper level of the transition (E_u/k); (6) and (7) the half-power beam-width (Θ_{mb}) and the main beam efficiency (η_{mb}) of the antenna. Further details of the SEST are available e.g. on the WWW at <http://www.ls.eso.org/lasilla/Telescopes/SEST>.

4. Results

4.1. Maps

The velocity-integrated HC₃N($J = 10 \rightarrow 9$) and SO($J_N = 4_3 \rightarrow 3_2$) line-intensity maps of Cha-MMS1 are presented in Fig. 1. The locations of the embedded infrared sources Ced 110 IRS2, IRS4 and IRS6 (Prusti et al. 1991), and the peak position of the 1.3 mm radio continuum source Cha-MMS1 (Reipurth et al. 1996) are also indicated. It is evident from the map that the HC₃N distribution is compact and peaks close to the dust continuum maximum, some $30''$ south of it. A comparison with Fig. 1 of Reipurth et al. 1996 shows that the dust continuum emission and the HC₃N line emission have similar sizes and shapes, and therefore conceivably originate from the same source, despite the slight shift in the peak positions. The infrared point sources lie near the northeastern edge of the molecular cloud core. SO line emission is present in the compact core, but shows no clear concentration. The maxima lie on its northern and southern sides, and are possibly related to a molecular outflow (see Sect. 5).

The integrated HNC($J = 1 \rightarrow 0$) and SO($J_N = 4_3 \rightarrow 3_2$) intensity maps of CrA C are shown in Fig. 2. In these

maps, the situation is the opposite of that in the maps of the Cha-MMS1 core. HNC, which was chosen instead of the undetected HC₃N, is weak and dispersed, whereas SO has a strong peak towards the offset ($30'', 30''$) from the centre of the map, and a weaker second maximum towards the offset ($60'', -30''$).

4.2. Spectra and line parameters

One location in each core was observed in several molecular transitions. In Cha-MMS1 this position lies towards the HC₃N peak at the offset ($-60'', -60''$), $17''$ southeast of the dust continuum peak. In CrA C the selected position lies close to the SO peak at the offset ($30'', 60''$) from the map centre, which has the highest SO line intensities. The spectra obtained towards these two locations are shown in Figs. 3 and 4.

In Cha-MMS1 all observed transitions except HC₃N($J = 15 \rightarrow 14$) were detected. The energy of the upper state of this transition is rather high (52 K) and so the non-detection of this line in a cold cloud is unsurprising. Since the SO lines were rather weak ($T_A^* \leq 0.7$ K) and showed no self-absorption features, ³⁴SO was not observed. In CH₃CCH, only the $K = 0$ and $K = 1$ components of the $J = 5 \rightarrow 4$ and $J = 8 \rightarrow 7$ transitions were clearly detected. The upper limits (3σ) for the $K=2$ and $K=3$ components are $T_A^*=0.063$ K ($J = 5 \rightarrow 4$) and $T_A^*=0.045$ K ($J = 8 \rightarrow 7$), respectively.

In CrA C, both of the observed SO transitions ($J_N = 3_2 \rightarrow 2_1$ and $4_3 \rightarrow 3_2$) were bright ($T_A^* > 1.5$ K). Only a tentative detection of HC₃N($J = 10 \rightarrow 9$) was made at a level of $T_A^*=0.05$ K, and so other transitions were not attempted. None of the CH₃CCH lines were detected, and the rest of the lines, both from carbonaceous species as well as from N₂H⁺, were weaker than in Cha-MMS1.

The common isotopomer HNC shows a broad, asymmetric profile. The fact that the peak is shifted with respect to the other lines, in particular that of HN¹³C, can be explained by absorption in the low density halo around the core. The larger width of this transition is partly due to the hyperfine structure discussed in Sect. 2.1. However, the broad wings visible on both sides of the line centre are not seen in any other line (including C¹⁸O). The presence of high velocity gas towards this location should be tested in other optically thick transitions.

In both clouds the C₃H₂($J_{K_a, K_c} = 3_{12} \rightarrow 2_{21}$) spectra also contain the $J_k = 3_{-1} \rightarrow 2_{-1} E$ and $J_k = 3_0 \rightarrow 2_0 A^+$ lines of CH₃OH. The former component appears in Figs. 3 and 4 as a negative spike due to the frequency switching procedure.

The observed line parameters (from fits of Gaussian line-profiles) in the selected positions are given in Table 4. We list the peak antenna temperatures (T_A^*), the

radial velocities (v_{LSR}), the full-width at half-maximum (FWHM) line-widths (Δv), and the velocity-integrated line-intensities ($\int T_{\text{A}}^* dv$) of the detected lines for both cores. For the undetected lines, the upper limits (3σ) for T_{A}^* are given.

4.3. Column densities

The method used in the calculation of the excitation temperatures, optical depths, and column densities is described in Appendix A. The results of this analysis are summarized in Table 5. The columns of this Table are: (1) the molecule; (2) the transition; (3), (4) and (5) the excitation temperature (T_{ex}) and the line-centre optical depth ($\tau_{\nu_{ul}}$) of the transition, and the total column density (N_{tot}) of the molecule in Cha-MMS1; (6), (7) and (8) T_{ex} , $\tau_{\nu_{ul}}$ and N_{tot} for the same molecule and transition in CrA C.

We have estimated the column densities of C^{18}O towards the centres of CrA C and Cha-MMS1 using data from Harju et al. 1993 and Haikala et al. 2000 (in preparation). Assuming optically thin line emission and a uniform excitation of the energy levels with $T_{\text{ex}} = 10$ K, we obtained $N(\text{C}^{18}\text{O}) \approx 3.1 \cdot 10^{15} \text{ cm}^{-2}$ in CrA C, and $N(\text{C}^{18}\text{O}) \approx 2.5 \cdot 10^{15} \text{ cm}^{-2}$ in Cha-MMS1. The two sources thus appear to have very similar C^{18}O column densities. The column densities of the observed molecules relative to C^{18}O are presented in Table 6. The conversion of the ratios listed in this Table to fractional abundances relative to H_2 is not trivial. The fractional CO abundance is expected and has also been observed to change from cloud to cloud. As discussed by Harjunpää & Mattila 1996 the fractional C^{18}O abundances can be different in star forming and non-star forming regions. The relations they derived towards the R CrA and the Cha I clouds (assuming $N(\text{H}_2)/E(J-K) = 5.4 \cdot 10^{21} \text{ cm}^{-2} \text{ mag}^{-1}$) give $2.4 \cdot 10^{22} \text{ cm}^{-2}$ and $1.2 \cdot 10^{22} \text{ cm}^{-2}$ for $N(\text{H}_2)$ in CrA C and Cha-MMS1, respectively. However, neither region studied by Harjunpää & Mattila 1996 in these complexes is actually close to our sources. The assumption that the relation they derived towards Coalsack is valid in the quiescent CrA C would result in an H_2 column density of $3.8 \cdot 10^{22} \text{ cm}^{-2}$. In comparison, the relation between $N(\text{H}_2)$ and $N(\text{C}^{18}\text{O})$ derived by Frerking et al. 1979 in Taurus yields $N(\text{H}_2) = 1.9 \cdot 10^{22} \text{ cm}^{-2}$ and $N(\text{H}_2) = 1.6 \cdot 10^{22} \text{ cm}^{-2}$ towards CrA C and Cha-MMS1, respectively. All these H_2 column densities are similar within a factor of two for each source, and so the values presented in Table 6 may be converted to approximate fractional abundances by multiplying them by 2×10^{-7} , bearing in mind that for CrA C, the value 1×10^{-7} is possibly more appropriate.

Table 6 shows that the column densities of carbon chain molecules (CCS, HC_3N , CH_3CCH and C_3H_2) relative to C^{18}O are much larger towards Cha-MMS1 than towards CrA C, for which upper limits only could be de-

rived for all species other than CCS. The $\text{HC}_3\text{N}/\text{C}^{18}\text{O}$ column density ratio towards Cha-MMS1 is almost 0.2, which implies that the fractional HC_3N abundance is of order 10^{-8} , being several times larger than towards the cyanopolyne maximum in TMC-1 (Pratap et al. 1997). The $\text{SO}/\text{C}^{18}\text{O}$ abundance ratio is larger towards CrA C. Inspection of the intensity ratios of the ^{34}SO and the normal isotope SO lines reveals that the latter are optically thick or even self-absorbed towards CrA C, and the derived SO column densities there are almost certainly lower limits (the terrestrial $^{32}\text{S}/^{34}\text{S}$ isotope ratio is 22.5 and in the local interstellar medium values larger than 10 are normally assumed). On the other hand, the $\text{N}_2\text{H}^+/\text{C}^{18}\text{O}$ column density ratio is a few times larger towards Cha-MMS1 than CrA C. Two molecules which have similar column densities towards both cores are C^{34}S and CH_3OH . For the rest of the molecules, the column densities relative to C^{18}O are so different in the two cores that despite the uncertainty concerning the $N(\text{H}_2)/N(\text{C}^{18}\text{O})$ conversion factor, this issue may be discussed below in terms of differences in fractional abundances.

Chemical differences between the two cores are manifest in Table 7, where we list the column density ratios of several molecules. The difference is most marked in the $\text{HC}_3\text{N}/\text{SO}$ column density ratio, which is at least three orders of magnitude higher towards Cha-MMS1 than CrA C. The ratios $\text{HC}_3\text{N}/\text{CCS}$ and $\text{HC}_3\text{N}/\text{N}_2\text{H}^+$ are more than a hundred times larger, and the $\text{C}^{34}\text{S}/^{34}\text{SO}$ ratio is about 30 times larger towards Cha-MMS1 than towards CrA C. However, the $\text{CCS}/\text{N}_2\text{H}^+$ column density ratio is similar towards both cores.

5. Discussion

In the previous Section it became evident that carbon-chain molecules are considerably more abundant in Cha-MMS1 than in CrA C, whereas the opposite is true for SO. In particular, the $\text{HC}_3\text{N}/\text{SO}$ column density ratio is at least 2000 times higher in Cha-MMS1 than in CrA C. The fact that HC_3N , CH_3CCH , $\text{c-C}_3\text{H}_2$ and CCS were detected without difficulty in one of the cores, but were all very weak or undetected in the other, is in agreement with the common belief that these species thrive in the same regions. For CCS, the difference in the abundances towards the two cores is the smallest for carbon-chain molecules, being ‘only’ about one order of magnitude.

As discussed in Sect. 2.2, time-dependent models of gas-phase chemistry suggest that HC_3N and other carbon-chain molecules reach their peak abundances at early stages of chemical evolution, whereas SO becomes abundant first at later times. Adopting this view, the $\text{HC}_3\text{N}/\text{SO}$ abundance ratios would indicate that Cha-MMS1 is chemically younger than CrA C. In addition, the CS/SO abundance ratio has been suggested to depend on the cloud age (Bergin & Langer 1997; Ruffle et al. 1999; Nilsson et al. 2000). Indeed, the CS/SO ratio is clearly

larger towards Cha-MMS1, which is mainly due to variation of the SO abundance, since the CS abundance is rather similar towards both cores.

On the other hand, it is difficult to understand in terms of pure gas-phase chemistry why CrA C has a higher SO abundance but a lower N_2H^+ abundance than Cha-MMS1: The production of N_2H^+ also increases first at later stages of chemical evolution. In particular, the fact that $\text{CCS}/\text{N}_2\text{H}^+$ column density ratio is similar towards both cores seems to contradict the expectation presented in Sect. 2.2 that this ratio could be usable as a chemical clock.

The inclusion of freezing-out of atoms, ions and molecules onto grain surfaces causes a complication for the time-dependence of molecular abundances. According to Ruffle et al. 1997, a second cyanopolyynes peak may occur when the depletion of gas-phase species becomes significant. The SO abundance also increases considerably at this time (Bergin & Langer 1997; Ruffle et al. 1999). In the models of Ruffle et al. 1999, the SO peak comes slightly *after* the second HC_3N peak (see their Figs. 1 and 2), probably because the C^+ abundance is then lower. After the SO peak, the dominant species in the gas phase are CO, CS and SO, until they too are depleted. It is uncertain how comparable the models of Bergin & Langer 1997 and Ruffle et al. 1999 are, however, since the former do not predict any late cyanopolyynes maximum.

N_2H^+ is included in the models of Rawlings et al. 1992 and Bergin & Langer 1997, where depletion onto grains are taken into account. In both models N_2H^+ shows a late peaking, and two reasons for this peaking are given. First, N_2 , which contributes to the N_2H^+ production, is only loosely bound in grain surfaces and returns quickly to the gas phase. Second, the drop in the gas-phase abundances of CO, H_2O and other neutral molecules with the advance of freezing-out decreases the destruction rate of N_2H^+ , until the electron recombination starts to dominate its removal.

Finally, it should be noted that nearby or embedded young stars may revive the ion-molecule chemistry in a dense core. As discussed by Hartquist et al. 1996, an intensified desorption of molecules from grain surfaces, the subsequent fragmentation of molecules into atoms in the gas-phase, and finally the ionization of atoms in a star-forming core may lead to increased abundances of C and C^+ . These could then re-start the synthesis of complex molecules, and accordingly the chemistry would have an ‘early-time’ character.

We have seen that chemistry models, regardless of whether they take accretion onto grains into account or not, predict that SO and N_2H^+ peak at late stages of chemical evolution, and that SO peaks later than HC_3N during the pre-stellar phase. Therefore, concerning the cores studied here, it is difficult to avoid the following conclusions: 1) CrA C has reached an advanced chemical stage. 2) Cha-MMS1 either represents the so called late-

time cyanopolyynes peak or a later stage where the chemistry has been influenced by neighbouring young stars.

The latter conclusion is based on the large N_2H^+ abundance in Cha-MMS1. Moreover, the interpretation that a collapsing cloud core containing a protostar, as Cha-MMS1 probably does, has reached the second, ‘late-time’ cyanopolyynes peak seems more natural than that it would represent ‘early-time’ chemistry, since such a core should exhibit a high degree of depletion (Rawlings et al. 1992; Bergin & Langer 1997). Possible outflows and radiation from the embedded protostar, IRS 10, or the other nearby protostars may have influenced the chemical composition of Cha-MMS1. Suzuki et al. 1992 found that NH_3 tends to be abundant in star-forming regions, and it seems possible that the production of NH_3 , and therefore also that of N_2H^+ (see Sect. 2), somehow depend on desorption processes. On the other hand, little time has passed since the collapse began (which should be coincident with the second cyanopolyynes peak) because the duration of the Class 0 phase is very short ($\sim 10^4$ years), and it is questionable whether the chemistry has really changed significantly during this time.

According to the models of Ruffle et al. 1999 and Bergin & Langer 1997, where the chemical development is coupled to kinematical models, the compositions observed in Cha-MMS1 and CrA C correspond to times a few million years after the initial state, which in these studies has been defined as a state where hydrogen is molecular but all other species are found as atoms or atomic ions. If the physical characteristics of the two cores were similar, Cha-MMS1 would not need to be much younger than CrA C. The latter core, however, appears to have a lower average density, and therefore the chemical evolution has probably been slower there. The result is surprising, since star-forming cores of the type Cha-MMS1 are normally expected to be older than starless cores like CrA C. Furthermore, previous observations have shown that the carbon-chain molecules are less abundant in star-forming regions than in quiescent clouds (Suzuki et al. 1992).

CrA C has been estimated to be gravitationally bound and therefore a potential site of star-formation (Harju et al. 1993). The present results indicate, however, that CrA C has existed long enough to reach an advanced chemical stage, which according to chemistry models implies a minimum age of $\sim 10^6$ years. This longevity raises doubts about the star-formation capacity of the core.

In quiescent cores, star formation occurs due to the cloud’s self-gravity, which has to work against the thermal pressure and the pressure and tension of the magnetic fields. Line emission from molecules, especially CO (as long as it is abundant in the gas phase), and collisions between gas and dust particles, can keep a cloud nearly isothermal even when contracting, and the importance of the magnetic support in weakly ionized cores has been recognized as the dominant factor preventing the collapse within the free-fall time, which in

the case of a dense core is of the order of 10^5 years. The magnetic support eventually gives way in the central parts of a core due to ambipolar diffusion, resulting in gravitational instability and collapse (Spitzer 1978; Mouschovias 1979; Lizano & Shu 1987). The density enhancement required for the gravitational collapse depends on the initial mass-to-magnetic-flux ratio. The rate at which the central density increases is related to the timescale of ambipolar diffusion (see e.g. Sect. 2 in Ciolek & Mouschovias 1993). The timescale of ambipolar diffusion in a dense core is proportional to the fractional ionization, and is typically of the order of 10^6 years (e.g. Spitzer 1978; Hartquist & Williams 1989). This time is shorter than the time needed for reaching a chemical equilibrium in pure gas-phase models, but comparable with the depletion timescale in models in which accretion onto grain surfaces are taken into account. According to Hartquist & Williams 1989, depletion can influence the dynamical state of a core, and in the extreme case, even prevent it from collapsing by causing an increase in the fractional ionization and removing coolants. Furthermore, as pointed out by Ciolek & Mouschovias (1993, 1994, 1995), the properties of dust grains can affect the ambipolar diffusion timescale and thus regulate the evolution of a core.

In simulations by Vanhala & Cameron 1997, the state of a gas-cloud first becomes non-adiabatic (i.e. the cloud is allowed to collapse) when its temperature has risen to about 27 K, at which point the rotational levels of H_2 become excited. Even though these authors use perhaps unrealistically low CO cooling efficiencies (they neglect the cooling below 10 K) this model may be qualitatively valid for very cold cores with highly reduced abundances of heavier molecules. If the temperature is too low, then the excitation is insufficient to provide strong enough line-emission, and a thermal balance is established. Hence, it may be that such cores have a poorer star-formation ability than previously supposed. Furthermore, an elevated temperature possibly is a useful diagnostic of the onset of a collapse, and could be used to identify dense pre-stellar cores that are close to forming stars.

Inferring from its chemical composition, the development in CrA C seem to have been very slow indeed, or then the gravitational forces in the core are simply balanced by thermal and magnetic pressures. In the ambipolar diffusion model the slow dynamical evolution could be explained by 1) a low initial mass-to-magnetic-flux ratio in the surrounding cloud; or 2) a high degree of ionization or a high fraction of charged dust grains, which both would lengthen the ambipolar diffusion timescale. The fact that the N_2H^+ abundance is lower in CrA C than in Cha-MMS1 suggests that the fractional ionization is indeed higher in the former. An alternative reason for the slow progress is that the cooling rate is very low in this core. Independent determinations of the kinetic temperature, the degree of ionization, and the degree of depletion towards

this core would certainly clarify this issue. Based on the results of coupled chemical and kinematical models (e.g. Rawlings et al. 1992; Bergin & Langer 1997), the high degree of depletion inferred from the molecular abundances implies a very advanced stage of evolution, and if the core is going to collapse, then this has already begun, or will do so soon deep in its interior parts. A search for infalling motions towards CrA C could be therefore profitable.

According to Lehtinen et al. 2000, the region of Cha-MMS1 may be an example of sequential star-formation, in which the core collapse is assisted by external forces such as stellar-winds originating from nearby young stars. This would conform with a rapid development, and may reflect favourable initial conditions for contraction and gravitational collapse in the parental cloud. In order to judge whether the chemistry in Cha-MMS1 is controlled by desorption or depletion, it would be useful to observe molecules which are predicted to increase in abundance when desorption mechanisms are effective. Our tentative column density estimates of CH_3OH (an example of such a molecule) did not, however, show any difference in relative abundances between CrA C and Cha-MMS1. Detailed chemistry models of the relative timing of the HC_3N , SO and N_2H^+ peaks would therefore be valuable.

The tiny SO maxima lying symmetrically on both sides of the HC_3N core in Cha-MMS1 (see Fig. 1) may be related to an outflow from the embedded protostar. These emission peaks and the Herbig-Haro object HH49/50 lie on the same line intersecting the centre of Cha-MMS1, and it seems that Cha-MMS1 can indeed be the driving source of HH49/50, as suggested by Reipurth et al. 1996. The stronger SO line emission towards the outflow axis may be understood in terms of an increased efficiency of neutral-neutral reactions involved in the formation of SO in shock-heated gas.

6. Conclusions

Comparison of observed molecular column densities and abundances in two dense cores, Cha-MMS1 and CrA C, reveal that they have very different chemical compositions, which according to time-dependent chemistry models can be interpreted as representing different stages of chemical evolution. Cha-MMS1, which is dynamically more evolved and contains a Class 0 protostar (Reipurth et al. 1996; Lehtinen et al. 2000), has large abundances of carbon-chain molecules. This is normally interpreted as a signature of an early stage of chemical evolution. In contrast, CrA C, which we suspected to be virginal and therefore a likely fund of ‘early type’ molecules, has, to all appearances, reached chemical maturity. This result seems to contradict the common assumption that star-forming cores are (chemically) older than starless cores. The chemical difference between the two cores is particularly pronounced in the HC_3N/SO abundance ratio, which is about 2000 times higher in Cha-MMS1 than in CrA C.

The fact that Cha-MMS1 has a large N_2H^+ abundance arouses doubts about its chemical youth, however. Namely, this molecular ion is formed from N_2 , which should become abundant only at later times. In fact, Cha-MMS1 probably represents the ‘late-time’ cyanopolyne peak predicted by Ruffle et al. 1997, which occurs when the freezing-out of molecules onto grain surfaces begins to be significant. Alternatively, the characteristics of youthful chemistry in Cha-MMS1 could have developed due to outflows and ionizing radiation from the embedded protostar or the neighbouring newly born stars. It should be noted, however, that these two alternatives do not have to lie very much apart in time. A high degree of depletion should be coincident with the collapse of the core nucleus (e.g. Rawlings et al. 1992; Bergin & Langer 1997), and Cha-MMS1 still contains a protostar in its main accretion phase. The fact that Cha-MMS1 is associated with a small cluster of young stars indicates a high star-formation efficiency in this region (Lehtinen et al. 2000), which would be consistent with a rapid collapse.

We have detected distinct SO emission maxima on both sides of Cha-MMS1, which may indicate the presence of a north-south oriented bipolar outflow. The suggestion by Reipurth et al. 1996 that Cha-MMS1 contains the central source of the Herbig-Haro object HH49/50 is strongly supported by the fact the SO peaks, Cha-MMS1 and HH49/50 lie along the same line.

The situation observed in CrA C, i.e. low abundances of carbon chain molecules and the large SO and N_2H^+ abundances, correspond to final stages of pure gas-phase chemistry evolution or to the ‘SO peak’ which comes after the late cyanopolyne peak in the model of Ruffle et al. 1999, in which gas-grain interactions has been taken into account. The lack of star-formation activity in the chemically ‘old’ core CrA C shows that the dynamical evolution has been slow there or that the core may have even reached an equilibrium. This may be due to a low mass-to-magnetic-flux ratio in the surrounding cloud, or a high degree of ionization or a high fraction of charged dust grains making the ambipolar diffusion time very long (e.g. Ciolek & Mouschovias 1994). On the other hand, insufficient cooling efficiency due to freezing-out of heavy molecules may have increased the thermal support.

Acknowledgements. We thank Lic. Päivi Harjunpää for discussions concerning the ‘LTE’ method applied here. We are grateful to Dr. Mark Rawlings, Dr. Malcolm Walmsley, Dr. Paola Caselli, and the referee, Dr. Glenn Ciolek, for very helpful comments on the manuscript. The work by S.K., J.H. and A.H. was supported by the Academy of Finland through grant No. 1011055. The Swedish-ESO Submillimetre Telescope is operated jointly by ESO and the Swedish National Facility for Radio Astronomy, Onsala Space Observatory at Chalmers University of Technology.

Table 1. Spectroscopic properties of the observed molecules.

Molecule	Type	μ_{electric} [Debye]	A [MHz]	B [MHz]	C [MHz]
SO	linear ($^3\Sigma$)	1.55	–	21 523.020	–
^{34}SO	linear ($^3\Sigma$)	1.55	–	21 102.720	–
C^{34}S	linear ($^1\Sigma$)	1.957	–	24 103.541	–
c- C_3H_2	asymmetric top (o/p)	3.43	35 092.6	32 212.8	16 749.1
CH_3OH	asymmetric top (A)	0.896	127 628.193	24 687.552	23 754.594
CH_3OH	asymmetric top (E)	0.896	127 628.7051	24 693.0658	23 757.1371
CCS	linear ($^3\Sigma$)	2.81	–	6 477.750	–
HC_3N	linear ($^1\Sigma$,hfs)	3.724	–	4 549.058	–
CH_3CCH	symmetric top (A/E)	0.75	158 590.0	8 545.86	8 545.86
HNC	linear ($^1\Sigma$,hfs)	3.05	–	45 331.990	–
HN^{13}C	linear ($^1\Sigma$,hfs)	2.699	–	43 545.61	–
N_2H^+	linear ($^1\Sigma$,hfs)	3.40	–	46 586.867	–

Table 2. Map centre coordinates and the positions selected for pointed observations.

Core	Map centre		Peak position	
	α	δ	$\Delta\alpha$	$\Delta\delta$
	(1950.0)			
Cha-MMS1	11 ^h 05 ^m 28 ^s .0	−77°06′32″	−60″	−60″
CrA C	19 ^h 00 ^m 33 ^s .2	−37°20′22″	30″	60″

Table 3. Observed transitions and some antenna parameters at their frequencies.

Frequency [MHz]	Molecule	Transition	S_{ul}	E_{u}/k [K]	Θ_{mb} [″]	η_{mb}
85 338.893	ortho-c- C_3H_2	$J_{K_a, K_c} = 2_{1,2} \rightarrow 1_{0,1}$	1.500	4.095 ^a	59	0.75
85 457.271	CH_3CCH	$J_K = 5_0 \rightarrow 4_0 A$	5.000	12.304	59	0.75
85 455.622	CH_3CCH	$J_K = 5_1 \rightarrow 4_1 E$	4.800	11.484 ^b	59	0.75
87 090.859	HN^{13}C	$J(F) = 1(2) \rightarrow 0(1)$	1.000 ^c	4.180	58	0.75
90 663.543	HNC	$J(F) = 1(2) \rightarrow 0(1)$	1.000 ^c	4.351	56	0.74
90 978.993	HC_3N	$J = 10 \rightarrow 9$	10.000	24.015	55	0.74
93 173.809	N_2H^+	$J(F_1, F) = 1(2, 3) \rightarrow 0(1, 2)$	1.000 ^c	4.472	54	0.74
93 870.023	CCS	$J_N = 8_7 \rightarrow 7_6$	7.971	19.892	54	0.74
96 412.940	C^{34}S	$J = 2 \rightarrow 1$	2.000	6.941	52	0.73
97 715.388	^{34}SO	$J_N = 3_2 \rightarrow 2_1$	2.935	9.100	52	0.73
99 299.879	SO	$J_N = 3_2 \rightarrow 2_1$	2.933	9.226	51	0.73
100 076.389	HC_3N	$J = 11 \rightarrow 10$	11.000	28.818	50	0.73
129 138.898	SO	$J_N = 3_3 \rightarrow 2_2$	2.670	25.511	39	0.68
135 775.633	^{34}SO	$J_N = 4_3 \rightarrow 3_2$	3.935	15.609	37	0.67
136 464.400	HC_3N	$J = 15 \rightarrow 14$	15.000	52.395	37	0.67
136 728.010	CH_3CCH	$J_K = 8_0 \rightarrow 7_0 A$	8.000	29.529	37	0.67
136 725.397	CH_3CCH	$J_K = 8_1 \rightarrow 7_1 E$	7.975	28.708 ^b	37	0.67
138 178.648	SO	$J_N = 4_3 \rightarrow 3_2$	3.938	15.857	36	0.67
144 617.109	C^{34}S	$J = 3 \rightarrow 2$	3.000	13.881	35	0.66
145 089.595	ortho-c- C_3H_2	$J_{K_a, K_c} = 3_{1,2} \rightarrow 2_{2,1}$	1.250	13.699 ^a	35	0.66
145 097.470	CH_3OH	$J_k = 3_{-1} \rightarrow 2_{-1} E$	2.667	11.607 ^b	35	0.66
145 103.230	CH_3OH	$J_k = 3_0 \rightarrow 2_0 A^+$	3.000	13.929	35	0.66

^a Relative to the ortho ground-state.^b Relative to the E -symmetry species ground-state.^c This value refers to the $J = 1 \rightarrow 0$ transition when all hfs components have been accounted for.

Table 4. Observational line parameters towards the centres of Cha-MMS1 and CrA C. The transitions are listed in the same order as in the figures showing the spectra.

Molecule	Transition	Cha-MMS1				CrA C			
		T_A^* [K]	v_{LSR} [km s ⁻¹]	Δv [km s ⁻¹]	$\int T_A^* dv$ [K km s ⁻¹]	T_A^* [K]	v_{LSR} [km s ⁻¹]	Δv [km s ⁻¹]	$\int T_A^* dv$ [K km s ⁻¹]
³⁴ SO	4 ₃ → 3 ₂	-	-	-	-	0.29±0.02	5.48±0.01	0.43±0.03	0.13±0.02
SO	4 ₃ → 3 ₂	0.37±0.04	4.35±0.02	0.55±0.04	0.21±0.04	1.44±0.04	5.43±0.01	0.56±0.01	0.87±0.04
SO	3 ₃ → 2 ₂	-	-	-	-	0.53±0.06	5.52±0.02	0.39±0.04	0.20±0.06
³⁴ SO	3 ₂ → 2 ₁	-	-	-	-	0.50±0.03	5.51±0.01	0.57±0.03	0.33±0.04
SO	3 ₂ → 2 ₁	0.70±0.02	4.37±0.01	0.74±0.02	0.56±0.03	1.79±0.05	5.43±0.01	0.70±0.02	1.40±0.06
C ³⁴ S	3 → 2	0.10±0.01	4.64±0.02	0.53±0.04	0.05±0.01	0.09±0.02	5.83±0.02	0.48±0.05	0.05±0.01
C ³⁴ S	2 → 1	0.22±0.01	4.66±0.01	0.63±0.03	0.14±0.01	0.23±0.01	5.89±0.01	0.62±0.03	0.16±0.02
CCS	8 ₇ → 7 ₆	0.31±0.02	4.15±0.01	0.65±0.03	0.21±0.02	0.07±0.01	5.40±0.03	0.38±0.06	0.03±0.02
o-c-C ₃ H ₂	3 _{1,2} → 2 _{2,1}	0.54±0.06	4.31±0.02	0.73±0.04	0.43±0.05	<0.26 ^a	-	-	-
o-c-C ₃ H ₂	2 _{1,2} → 1 _{0,1}	1.24±0.02	4.32±0.01	0.82±0.01	1.09±0.02	0.15±0.01	5.63±0.01	0.38±0.03	0.07±0.01
CH ₃ OH	3 ₋₁ → 2 _{-1 E}	0.42±0.03	4.46±0.01	0.62±0.02	0.28±0.03	0.61±0.03	5.63±0.01	0.53±0.01	0.34±0.03
CH ₃ OH	3 ₀ → 2 _{0 A⁺}	0.48±0.03	4.46±0.01	0.62±0.02	0.32±0.03	0.79±0.03	5.63±0.01	0.53±0.01	0.44±0.03
HN ¹³ C	1 → 0	-	-	-	-	0.09±0.01	5.70±0.03	0.76±0.08	0.07±0.02
HNC	1 → 0	-	-	-	-	0.63±0.05 ^b	5.21±0.02 ^b	0.65±0.01 ^b	0.57±0.06
HC ₃ N	15 → 14	< 0.13 ^a	-	-	-	-	-	-	-
HC ₃ N	11 → 10	0.57±0.03	4.39±0.01	0.74±0.03	0.47±0.04	-	-	-	-
HC ₃ N	10 → 9	0.85±0.02	4.36±0.01	0.65±0.01	0.59±0.03	0.04±0.01	5.23±0.04	0.34±0.09	0.02±0.01
CH ₃ CCH	8 ₀ → 7 ₀	0.20±0.02	4.53±0.02	0.58±0.04	0.12±0.02	<0.083 ^a	-	-	-
CH ₃ CCH	8 ₁ → 7 ₁	0.16±0.02	4.49±0.02	0.52±0.04	0.08±0.02	<0.083 ^a	-	-	-
CH ₃ CCH	5 ₀ → 4 ₀	0.43±0.01	4.41±0.01	0.63±0.02	0.30±0.03	<0.071 ^a	-	-	-
CH ₃ CCH	5 ₁ → 4 ₁	0.39±0.01	4.41±0.01	0.62±0.02	0.26±0.02	<0.071 ^a	-	-	-
N ₂ H ⁺	1 → 0	1.67±0.03	4.57±0.01	0.63±0.01	5.02±0.03	0.45±0.02	5.77±0.01	0.46±0.01	0.94±0.03

^a 3 σ .

^b Applies for the strongest component in the spectrum.

Table 5. The excitation temperatures and the line-centre optical depths of the observed transitions, and the total molecular column densities towards the peak positions of Cha-MMS1 and CrA C.

Molecule	Transition	Cha-MMS1			CrA C		
		T_{ex} [K]	$\tau_{\nu_{\text{ul}}}$	N_{tot} [cm ⁻²]	T_{ex} [K]	$\tau_{\nu_{\text{ul}}}$	N_{tot} [cm ⁻²]
³⁴ SO	4 ₃ → 3 ₂	-	-	-	3.9±0.1	0.69±0.01	1.9±0.1 · 10 ¹³
SO	4 ₃ → 3 ₂	4.4±0.1	0.59±0.07	2.0±0.2 · 10 ¹³	5.8±0.9	2.10±0.70	6.6±2.3 · 10 ¹³
SO	3 ₃ → 2 ₂	-	-	-	5.8±0.9	0.37±0.05	7.2±2.2 · 10 ¹³
³⁴ SO	3 ₂ → 2 ₁	-	-	-	3.9±0.1	1.16±0.01	2.0±0.1 · 10 ¹³
SO	3 ₂ → 2 ₁	4.4±0.1	1.10±0.20	2.7±0.3 · 10 ¹³	5.8±0.9	2.30±0.90	6.7±2.7 · 10 ¹³
C ³⁴ S	3 → 2	3.3±0.1	0.49±0.04	5.7±0.5 · 10 ¹²	3.4±0.1	0.38±0.04	3.9±0.5 · 10 ¹²
C ³⁴ S	2 → 1	3.3±0.1	1.00±0.10	5.7±0.6 · 10 ¹²	3.4±0.1	0.83±0.12	5.0±0.7 · 10 ¹²
CCS	8 ₇ → 7 ₆	4±1 ^a	-	3.1±0.3 · 10 ¹³	4±1 ^a	-	4.0±2.0 · 10 ¹²
o-c-C ₃ H ₂	3 _{1,2} → 2 _{2,1}	4.7±0.2	0.83±0.14	4.7±0.8 · 10 ¹³	-	-	-
o-c-C ₃ H ₂	2 _{1,2} → 1 _{0,1}	4.7±0.2	2.80±1.60	4.7±2.7 · 10 ¹³	4±1 ^a	-	1.2±0.2 · 10 ¹²
CH ₃ OH	3 ₋₁ → 2 _{-1 E}	4±1 ^a	-	6.8±1.3 · 10 ¹³	4±1 ^a	-	8.0±2.0 · 10 ¹³
CH ₃ OH	3 ₀ → 2 _{0 A⁺}	4±1 ^a	-	1.2±0.2 · 10 ¹⁴	4±1 ^a	-	1.7±0.3 · 10 ¹⁴
HN ¹³ C	1 → 0	-	-	-	4±1 ^a	-	3.2±0.7 · 10 ¹¹
HNC	1 → 0	-	-	-	4±1 ^a	-	2.0±0.1 · 10 ¹²
HC ₃ N	11 → 10	4.1±0.1	1.10±0.20	4.5±0.8 · 10 ¹⁴	-	-	-
HC ₃ N	10 → 9	4.1±0.1	3.00±2.00	4.5±2.5 · 10 ¹⁴	6±1 ^a	-	< 5.7 · 10 ¹¹ ^b
CH ₃ CCH	8 ₀ → 7 ₀	9.9±0.8	0.05±0.01	1.1±0.2 · 10 ¹⁴	-	-	-
CH ₃ CCH	8 ₁ → 7 ₁	8.5±0.8	0.05±0.01	1.0±0.2 · 10 ¹⁴	-	-	-
CH ₃ CCH	5 ₀ → 4 ₀	9.9±0.8	0.09±0.01	1.1±0.2 · 10 ¹⁴	-	-	-
CH ₃ CCH	5 ₁ → 4 ₁	8.5±0.8	0.10±0.01	1.0±0.2 · 10 ¹⁴	-	-	-
N ₂ H ⁺	1 → 0	4±1 ^a	-	1.4±0.1 · 10 ¹³	4±1 ^a	-	2.6±0.1 · 10 ¹²

^a The excitation temperature has been assumed.

^b The rms is so large compared to the line intensity that only a upper limit for the column density is given here.

Table 6. Column densities relative to C¹⁸O*.

Molecules	Cha-MMS1	CrA C
	$N_{\text{tot}}/N_{\text{C}^{18}\text{O}} (\times 10^3)$	$N_{\text{tot}}/N_{\text{C}^{18}\text{O}} (\times 10^3)$
³⁴ SO	-	6.3 ± 0.5
SO	8.0 ± 1.0	22 ± 8
C ³⁴ S	2.3 ± 0.3	1.3 ± 0.2
CCS	12 ± 2	1.3 ± 0.7
o-c-C ₃ H ₂	19 ± 4	< 0.4
CH ₃ OH	27 ± 6	27 ± 7
HN ¹³ C	-	0.11 ± 0.02
HNC	-	0.67 ± 0.06
HC ₃ N	180 ± 35	< 0.2
CH ₃ CCH	44 ± 9	-
N ₂ H ⁺	5.6 ± 0.6	0.87 ± 0.07

* The C¹⁸O/H₂ column density ratio is normally assumed to be about $2 \cdot 10^{-7}$. In quiescent regions like CrA C this ratio can be, however, lower by a factor of two (Harjunpää & Mattila 1996).

Table 7. Column density ratios.

Molecules	Cha-MMS1	CrA C
HC ₃ N / CCS	15 ± 3	< 0.14
HC ₃ N / SO	23 ± 5	< 0.01
HC ₃ N / N ₂ H ⁺	32 ± 6	< 0.22
HC ₃ N / CH ₃ CCH	4 ± 1	-
HC ₃ N / C ₃ H ₂	10 ± 3	< 0.48
C ³⁴ S / ³⁴ SO	$6.4 \pm 0.9^{\text{a}}$	0.21 ± 0.03
N ₂ H ⁺ / SO	0.7 ± 0.1	0.04 ± 0.01
CCS / N ₂ H ⁺	2.2 ± 0.3	1.5 ± 0.8
C ³⁴ S / N ₂ H ⁺	0.41 ± 0.05	1.5 ± 0.2

^a The ³²S/³⁴S isotope ratio is assumed to be 22.5.

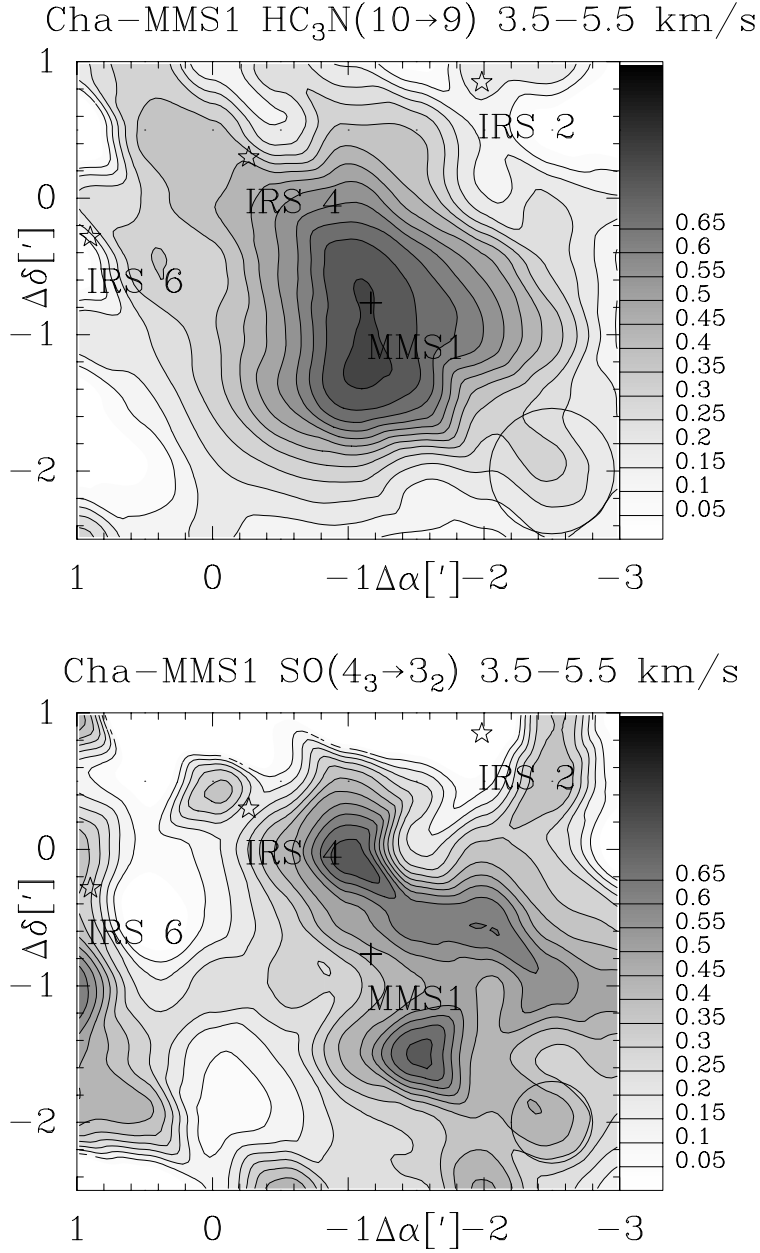


Fig. 1. The $\text{HC}_3\text{N}(J = 10 \rightarrow 9)$ and $\text{SO}(J_N = 4_3 \rightarrow 3_2)$ integrated intensity ($\int T_{\text{A}}^* dv$) maps of Cha-MMS1. The velocity range and the intensity levels (in K km s^{-1}) are indicated in the Figure. Typical 3σ rms noise levels are 0.04 K km s^{-1} and 0.11 K km s^{-1} in the HC_3N and the SO maps, respectively. The locations of the 1.3 mm dust continuum peak MMS1 (Reipurth et al. 1996), and the nearest embedded infrared sources (Prusti et al. 1991) are denoted by a cross and stars, respectively. The beamsizes are indicated in the bottom right of each map. The coordinates of the (0,0) position are given in Table 2.

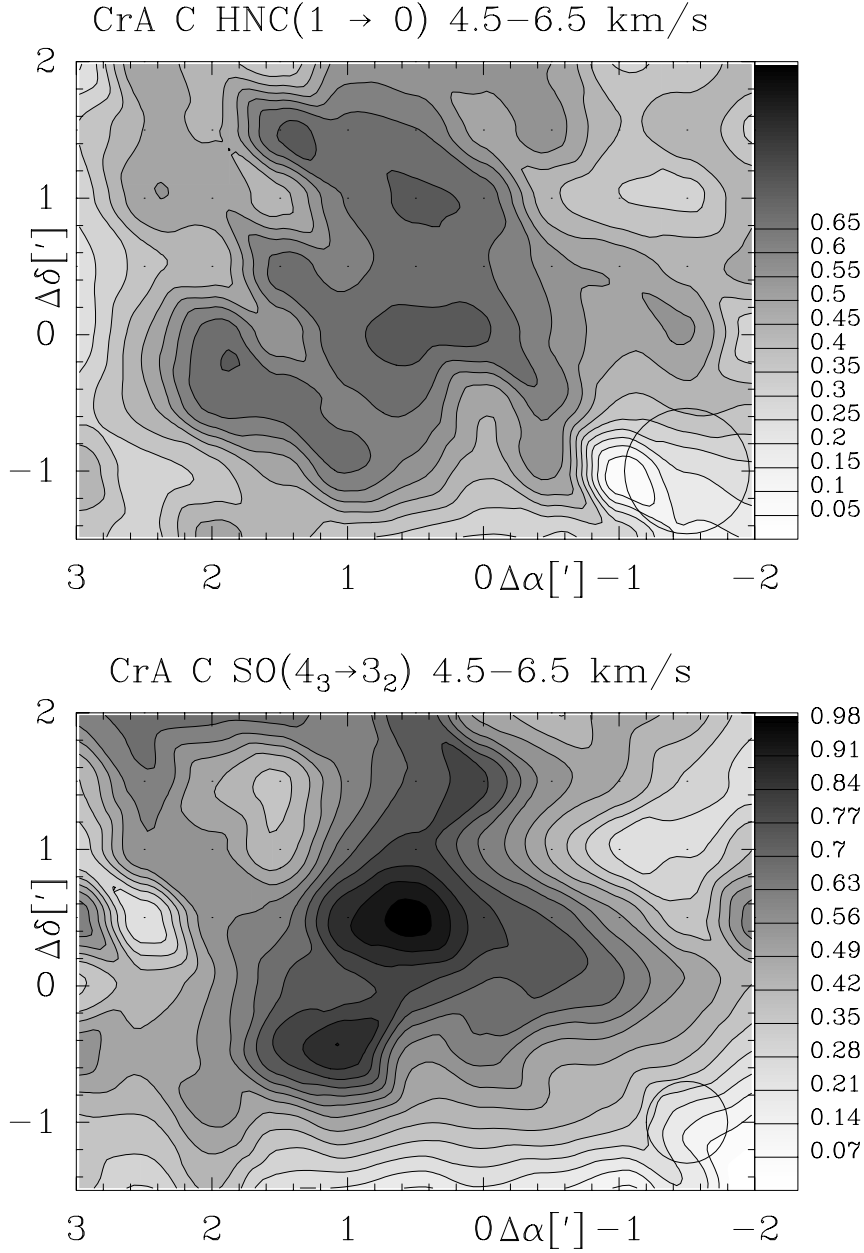


Fig. 2. The HNC($J = 1 \rightarrow 0$) and SO($J_N = 4_3 \rightarrow 3_2$) integrated intensity ($\int T_A^* dv$) maps of CrA C. The velocity range and the intensity levels (in K km s^{-1}) are indicated in the Figure. Typical 3σ rms noise levels are 0.06 K km s^{-1} and 0.11 K km s^{-1} in the HNC and the SO maps, respectively. The beamsizes are indicated in the bottom right of each map, and the coordinates of the (0,0) position are given in Table 2.

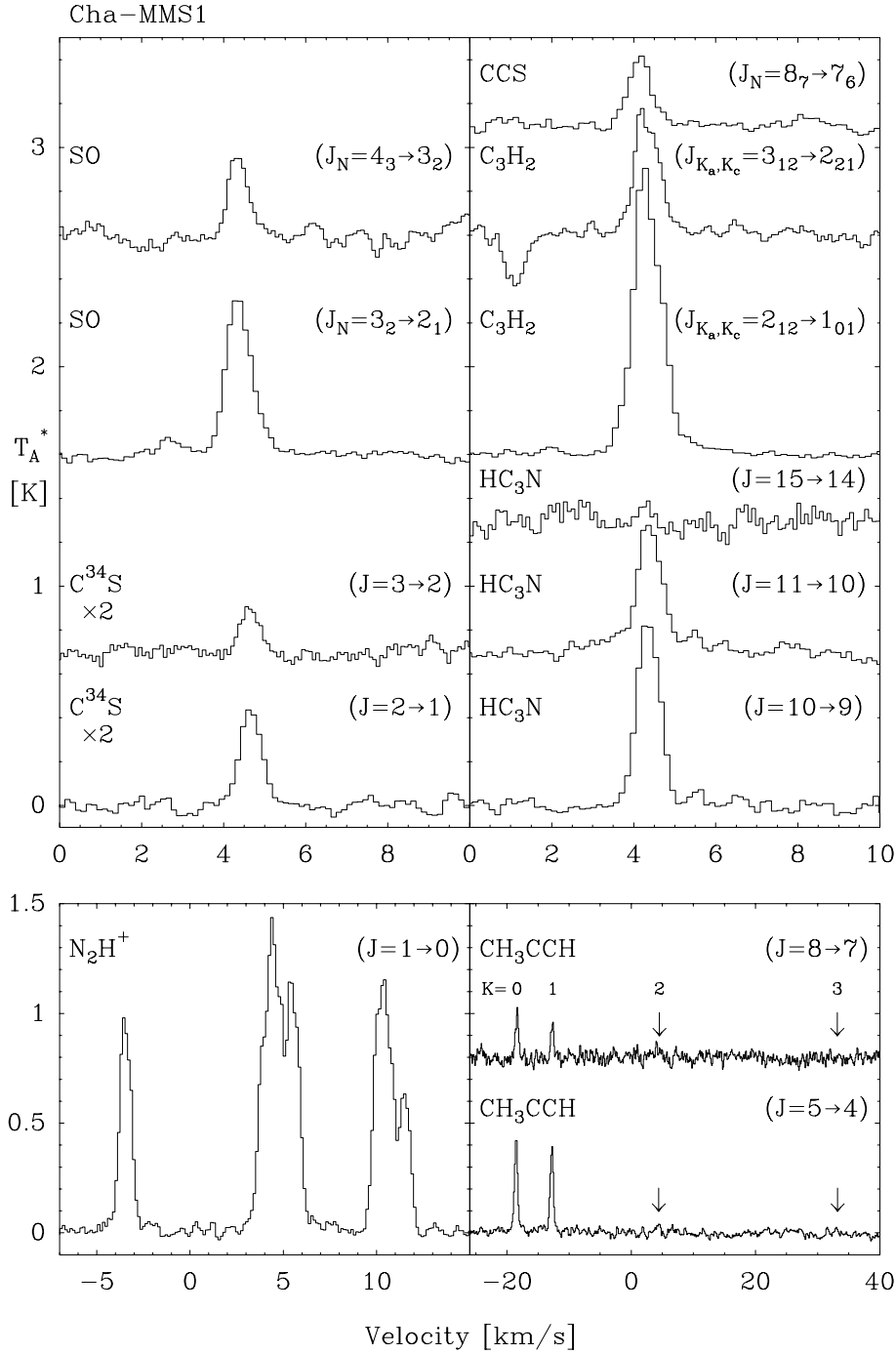


Fig. 3. The observed spectra towards the centre of Cha-MMS1. The spectra are in the T_A^* scale and the velocity in relative to the local standard of rest. The upper panel shows the lines observed using frequency switching, while the lower panel shows the position switched spectra. Note the different velocity ranges. The intensity in the $C^{34}S$ spectra are multiplied by a factor of two. The feature showing a negative intensity in the C_3H_2 ($J_{K_a, K_c} = 3_{1,2} \rightarrow 2_{2,1}$) spectrum is caused by the $J_k = 3_0 \rightarrow 2_0 A^+$ line of CH_3OH , which lies close in the frequency. The frequency switching method causes the line to appear with a negative intensity. The CH_3CCH spectra are centered on the $K = 2$ components, which, however, remain undetected. The locations of the $K = 0, 1, 2$ and 3 components are marked by arrows.

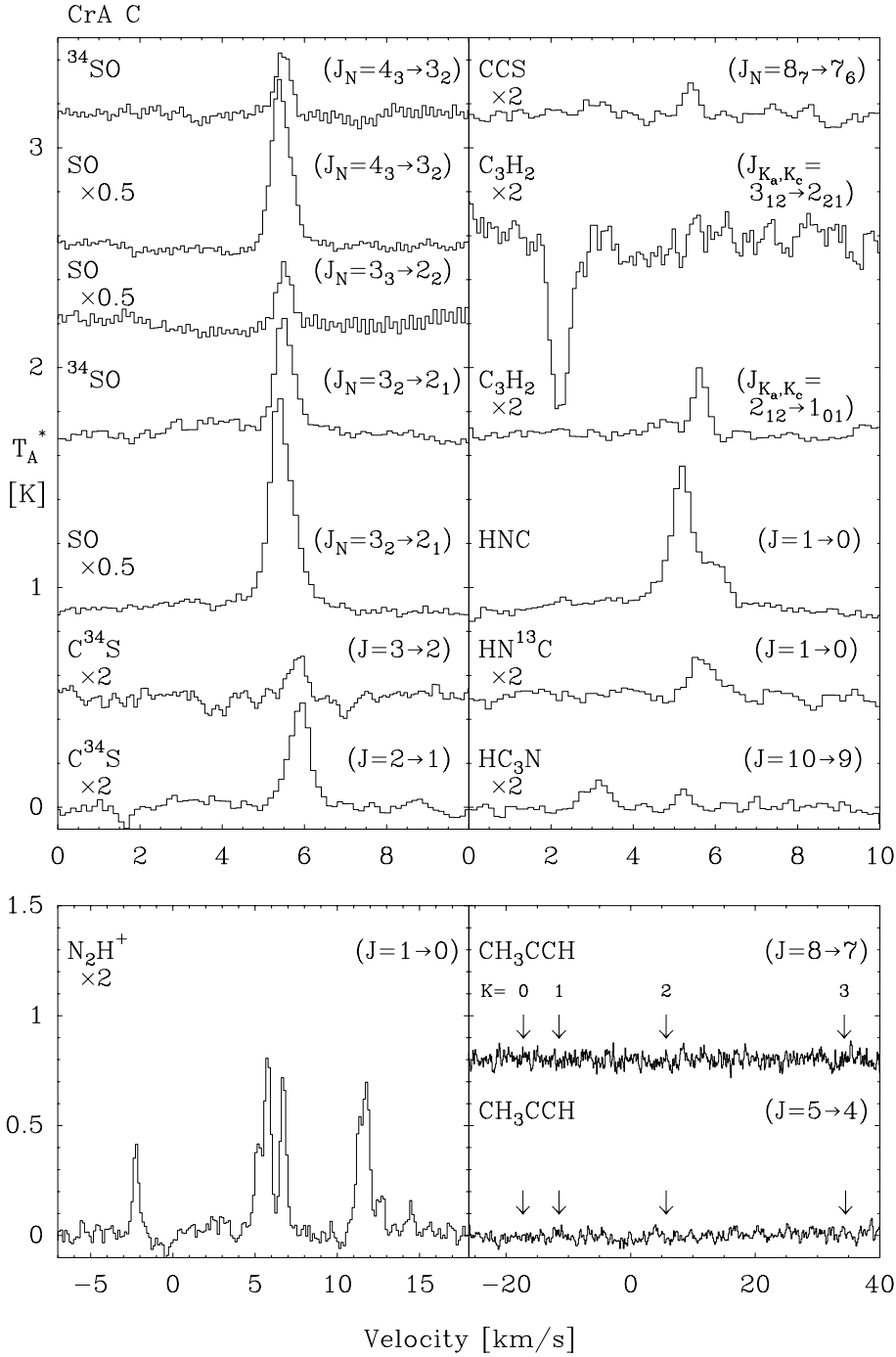


Fig. 4. The observed spectra towards the centre of CrA C. The spectra are in the T_A^* scale and the velocity in relative to the local standard of rest. As for Cha-MMS1, the frequency switched and position switched spectra are placed into different boxes. The selection of transitions is, however, slightly different. Note that many of the spectra are either multiplied or divided by a factor of two. The $\text{C}_3\text{H}_2(J_{K_a, K_c} = 3_{12} \rightarrow 2_{21})$ spectrum contains the negative ‘ CH_3OH feature’. In the CH_3CCH spectra we have marked the positions where the $K = 0, 1, 2$ and 3 components should lie.

Appendix A: Formulae used in the excitation temperature and column density calculations

The excitation temperatures (T_{ex}) and molecular column densities (N_{tot}) were estimated using a local thermodynamic equilibrium (LTE) approach in the sense that we assume a uniformly excited and Boltzmann distributed population of the energy levels for the molecule question. However, we refrain from making any assumptions concerning the (line-centre) optical depths ($\tau_{\nu_{\text{ul}}}$). Instead we derive an exact equation (A5 below) for a two-level system, from which T_{ex} can be determined numerically (see Nummelin et al. 2000 for an LTE treatment of the excitation of molecules with numerous observed lines with no a priori assumptions about the optical depths).

By assuming that $\tau_{\nu_{\text{ul}}}$ has a gaussian velocity distribution, the formal definition of the optical depth leads to the following expression for its value at the line-centre:

$$\tau_{\nu_{\text{ul}}} = 10^{-41} \sqrt{\frac{\ln 2}{\pi}} \frac{16\pi^3}{3h} \frac{\mu_{\text{el}}^2 S_{\text{ul}} g(I, K) N_{\text{tot}}}{Q(T_{\text{ex}}) \Delta v} \times \exp(-E_{\text{u}}/kT_{\text{ex}}) (\exp(h\nu_{\text{ul}}/kT_{\text{ex}}) - 1). \quad (\text{A1})$$

The factor 10^{-41} stems from using Debye and kms^{-1} as the units for the electric dipole moment (μ_{el}) and the FWHM line-width (Δv), respectively. Quantities related to the observed transition are: the rest-frequency ν_{ul} [Hz], the line-strength S_{ul} , and the energy of the upper level E_{u} . Furthermore, N_{tot} is the total column density [cm^{-2}], $Q(T_{\text{ex}})$ is the partition function, $g(I, K)$ is the statistical weight due to possible nuclear spin and K -degeneracy, and h and k are the Planck and Boltzmann constants (given in cgs-units), respectively.

A second expression for $\tau_{\nu_{\text{ul}}}$ is obtained from the ‘‘antenna equation’’:

$$T_{\text{R}} = \frac{h\nu_{\text{ul}}}{k} [F(\nu_{\text{ul}}, T_{\text{ex}}) - F(\nu_{\text{ul}}, T_{\text{bg}})] [1 - \exp(-\tau_{\nu_{\text{ul}}})] \quad (\text{A2})$$

where

$$F(\nu_{\text{ul}}, T) = \frac{1}{\exp(h\nu_{\text{ul}}/kT) - 1}. \quad (\text{A3})$$

T_{B} is the brightness temperature calculated from the observed T_{A}^* by correcting for relevant beam-efficiencies and beam-filling factors. In the analysis of the observational data, we used the main-beam brightness temperature ($T_{\text{mb}} = T_{\text{A}}^*/\eta_{\text{mb}}$), assumed the beam-filling to be one for all lines, and did not introduce any corrections due to different beam sizes.. T_{bg} is the temperature of the background radiation (here taken as a black-body at a temperature of 2.728 K).

Eqs.(A2 and A3) yield:

$$\tau_{\nu_{\text{ul}}} = \ln \left[\frac{[F(\nu_{\text{ul}}, T_{\text{ex}}) - F(\nu_{\text{ul}}, T_{\text{bg}})]}{[F(\nu_{\text{ul}}, T_{\text{ex}}) - F(\nu_{\text{ul}}, T_{\text{bg}})] - \frac{kT_{\text{B}}}{h\nu_{\text{ul}}}} \right]. \quad (\text{A4})$$

Combining the Eqs. (A1 and A4) and re-arranging the terms leads to an expression, which besides T_{ex} contains only known constants or observed quantities. By applying this to two spectral lines of the same molecule, and taking the ratio of the resulting expressions, the final equation for T_{ex} reads:

$$\begin{aligned} \ln \left[\frac{[F(\nu_2, T_{\text{ex}}) - F(\nu_2, T_{\text{bg}})]}{[F(\nu_2, T_{\text{ex}}) - F(\nu_2, T_{\text{bg}})] - \frac{kT_{\text{B},2}}{h\nu_2}} \right] \frac{F(\nu_2, T_{\text{ex}})}{F(\nu_1, T_{\text{ex}})} \exp\left(\frac{E_{\text{u},2} - E_{\text{u},1}}{kT_{\text{ex}}}\right) \\ \ln \left[\frac{[F(\nu_1, T_{\text{ex}}) - F(\nu_1, T_{\text{bg}})]}{[F(\nu_1, T_{\text{ex}}) - F(\nu_1, T_{\text{bg}})] - \frac{kT_{\text{B},1}}{h\nu_1}} \right] \\ = \frac{\Delta v_1 S_{\text{ul},2}}{\Delta v_2 S_{\text{ul},1}}. \end{aligned} \quad (\text{A5})$$

The subscripts ‘‘1’’ and ‘‘2’’ refer to ‘‘line 1’’ and ‘‘line 2’’, respectively. Terms involving T_{ex} have been collected on the left hand side of this expression. We solved Eq.(A5) for given observed line parameters by searching through a sufficiently large T_{ex} interval. When applying this equation to the observed data, we found that in addition to the case with a single unique solution, there are also cases where no solution exists, as well as cases where two solutions are present. The lack of solutions indicates that the assumption of a uniform T_{ex} for both transitions has been violated or that the beam-filling factors of the two transitions are different; in this case we have chosen the point where we have the least deviation from a solution as the value for T_{ex} . The case with two solutions manifestates itself by giving one solution with a low T_{ex} and high $\tau_{\nu_{\text{ul}}}$, the second solution having a higher T_{ex} and lower $\tau_{\nu_{\text{ul}}}$. In the analysis we have chosen to use the low T_{ex} - high $\tau_{\nu_{\text{ul}}}$ alternative.

Once T_{ex} was estimated, $\tau_{\nu_{\text{ul}}}$ was calculated from Eq.(A4) and subsequently N_{tot} was derived from Eq.(A1).

In cases where we have only one observed transition, we have assigned a T_{ex} close to that of a species with similar excitation requirements. N_{mol} is then obtained, assuming optically thin emission, from the formula:

$$N_{\text{tot}} = \frac{1.67 \cdot 10^{23} \exp(E_{\text{u}}/kT_{\text{ex}}) Q(T_{\text{ex}}) I_{\text{line}}}{\left(1 - \frac{F(T_{\text{bg}})}{F(T_{\text{ex}})}\right) \nu \mu_{\text{el}}^2 S_{\text{ul}} g(I, K)}. \quad (\text{A6})$$

Here $I_{\text{line}} = \int T_{\text{B}} dv$ is the velocity-integrated line-intensity [K km s^{-1}].

In the calculation of the column densities the partition functions need to be evaluated. For lin-

ear rotors ($^1\Sigma$) we used the following formula (e.g. Townes & Schawlow 1975, chapter 1):

$$Q \approx \frac{kT_{\text{ex}}}{hB} + \frac{1}{3} \quad (\text{A7})$$

where B is the rotation constant.

For CCS and SO we made a direct summation over the energy levels with $E_i/k < 575$ K:

$$Q = \sum_i g_i \exp(-E_i/kT_{\text{ex}}) \quad (\text{A8})$$

where g_i is the statistical weight, $2J_i + 1$, with the relevant J_i used.

We would like to emphasize that the evaluation of the partition function through direct summation is essential in the case of SO and CCS. For example for SO, the ‘‘usual’’ integral approximation of the partition function ($3 \frac{kT_{\text{ex}}}{hB} - 1$) overestimates Q by a factor of 1.1 to 1.85 in the temperature range 2–70 K; the largest discrepancy occurs at $T_{\text{ex}} \approx 5$ K. Thus for SO this simple approximation can be used only for temperatures above 80 K or so. A better analytical approximation for Q at temperatures below 80 K can be obtained by treating each of the three N ladders as separate rigid rotors and integrating over J . Note that only one of the ladders ($J = N - 1$) has $J=0$ as its lowest level; the two other ladders begin with $J=1$. The resulting partition functions are:

$$Q_{J=N-1,\text{ladder}} \approx \frac{kT_{\text{ex}}}{hB} + \frac{1}{3} \quad (\text{A9})$$

$$Q_{J=N,\text{ladder}} \approx \left(\frac{kT_{\text{ex}}}{hB} - \frac{2}{3} \right) \exp(-\Delta E_1/kT_{\text{ex}}) \quad (\text{A10})$$

$$Q_{J=N+1,\text{ladder}} \approx \left(\frac{kT_{\text{ex}}}{hB} - \frac{2}{3} \right) \exp(-\Delta E_2/kT_{\text{ex}}) \quad (\text{A11})$$

where ΔE_1 is the energy difference between the lowest levels in the $J = N$ and $J = N - 1$ ladders, and ΔE_2 the corresponding difference between the $J = N + 1$ and $J = N - 1$ ladders. The lowest states in these ladders are $J_N=0_1$ (the ground-state), 1_1 , and 1_0 , respectively.

The total partition function is then:

$$Q = Q_{J=N-1,\text{ladder}} + Q_{J=N,\text{ladder}} + Q_{J=N+1,\text{ladder}}. \quad (\text{A12})$$

For SO, this approximation overestimates the true partition function by less than 15% for temperatures between 3 and 80 K, the error being less than 5% for $T_{\text{ex}} > 25$ K. The values for ΔE_1 and ΔE_2 are 15.18 K and 1.44 K (SO); 9.33 K and 0.53 K (CCS), respectively.

For c-C₃H₂ we used:

$$Q \approx 2\sqrt{\frac{\pi k^3 T_{\text{ex}}^3}{h^3 ABC}} \approx 2.450 T_{\text{ex}}^{3/2}. \quad (\text{A13})$$

The contributions from both ortho- and para-states have been accounted for by taking into account their different statistical weights: 3 for ortho and 1 for para.

For CH₃OH we used:

$$Q \approx 2\sqrt{\frac{\pi k^3 T_{\text{ex}}^3}{h^3 ABC}} \approx 1.232 T_{\text{ex}}^{3/2}. \quad (\text{A14})$$

The (equal) contributions from both the A - and the E -symmetry species have been accounted for.

For CH₃CCH it is common to use the expression:

$$Q \approx \frac{8}{3}\sqrt{\frac{\pi k^3 T_{\text{ex}}^3}{h^3 ABC}} \approx 4.177 T_{\text{ex}}^{3/2}. \quad (\text{A15})$$

where the contributions from both the A - and the E -symmetry species have been accounted for by taking into consideration the spin statistics of the various levels (see e.g. Townes & Schawlow 1975, chapter 3).

However, Eq.(A15) is valid only at high enough temperatures. Since the lines observed by have low excitation temperatures, we derived a more accurate approximation for temperatures below 30 K. Each K -ladder was treated as a linear rotor and the integration was performed over J . Note that $J=K$ is the lowest level of a specific K -ladder. By taking into account only the three first ladders ($K=0, 1, 2$) we have:

$$Q_{K=0,\text{ladder}} \approx \frac{kT_{\text{ex},J}}{hB} + \frac{4}{3} \quad (\text{A16})$$

$$Q_{K=1,\text{ladder}} \approx \left(\frac{kT_{\text{ex},J}}{hB} - \frac{8}{3} \right) \exp(-\Delta E_3/kT_{\text{ex},K}) \quad (\text{A17})$$

$$Q_{K=2,\text{ladder}} \approx \left(\frac{kT_{\text{ex},J}}{hB} - \frac{8}{3} - 12 \exp(-\Delta E_3/kT_{\text{ex},J}) \right) \times \exp(-\Delta E_4/kT_{\text{ex},K}) \quad (\text{A18})$$

where $\Delta E_3/k \approx 7.20$ K and $\Delta E_4/k \approx 28.80$ K are the energy differences between the lowest levels of the $K=1$ and $K=2$ ladders, respectively, relative to the $K=0$ ladder. $T_{\text{ex},J}$ is the excitation temperature along a specific K -ladder (i.e. K fix, J varies), and $T_{\text{ex},K}$ is the excitation temperature between different K -ladders (i.e. K varies, J fix).

The resulting expression for the total partition function for CH₃CCH, which in the indicated temperature range underestimates the result from a direct summation by less than 10%, is given by:

$$Q \approx Q_{K=0,\text{ladder}} + Q_{K=1,\text{ladder}} + Q_{K=2,\text{ladder}} \quad (\text{A19})$$

References

- Anderson T., De Lucia F.C., Herbst E. 1990, ApJS 72, 797
- Benson P.J., Caselli P., Myers P.C. 1998, ApJ 506, 743
- Bergin E.A., Langer W.D. 1997, ApJ 486, 316
- Bergin E.A., Goldsmith P.F., Snell R.L., Ungerechts H. 1994, ApJ 431, 674
- Caselli P., Myers P.C., Thaddeus P. 1995, ApJ 455, L77
- Ciolek G.E., Mouschovias T.C. 1993, ApJ 418, 774
- Ciolek G.E., Mouschovias T.C. 1994, ApJ 425, 142
- Ciolek G.E., Mouschovias T.C. 1995, ApJ 454, 194
- Cox P., Walmsley C.M., Güsten R. 1989, A&A 209, 382
- Gordy W., Cook R.L. 1970, *Microwave Molecular Spectra*, John Wiley & Sons, Inc., New York
- Federman S.R., Huntress W.T., Jr., Prasad S.S. 1990, ApJ 354, 504
- Frerking M.A., Langer W.D., Wilson R.W. 1979, ApJ 232, L65
- Harju J., Haikala L.K., Mattila K., et al. 1993, A&A 278, 569
- Harjunpää P., Mattila K. 1996, A&A 305, 920
- Hartquist T.W., Williams D.A. 1989, MNRAS 241, 417
- Hartquist T.W., Williams D.A., Caselli P. 1996, Ap&SS 238, 303
- Herbst E. 1978, ApJ 222, 508
- Herbst E., Leung C.M. 1989, ApJS 69, 271
- Hirahara Y., Suzuki H., Yamamoto S., et al. 1992, ApJ 394, 539
- Hirahara Y., Masuda A., Kawaguchi K., et al. 1995, PASJ 47, 1
- Huntress W.T. Jr., Mitchell G.F. 1979, ApJ 231, 456
- Knude J., Høg E. 1998, A&A 338, 897
- Lehtinen K., Haikala L.K., Mattila K., Lemke D. 2000, *submitted to A&A*
- Little L.T., MacDonald G.H., Riley P.W., Matheson D.N. 1979, MNRAS 189, 539
- Lizano S., Shu F.H. 1987, in *Physical Processes in Interstellar Clouds*, Eds. Morfill G.E., Scholer M., D.Reidel, Dordrecht, Holland, p. 173
- Llewellyn R., Payne P., Sakellis S., Taylor K.N.R., 1981, MNRAS 196, 29P
- Mattila K., Liljeström T., Toriseva M. 1989, in *Low Mass Star Formation and Pre-Main Sequence Objects*, Reipurth B. (ed.), ESO Conference and Workshop Proceedings 33, p. 153
- Menten K.M., Walmsley C.M., Henkel C., Wilson T.L. 1988, A&A 198, 253
- Mouschovias T.C. 1979, ApJ 228, 475
- Murukami A. 1990, ApJ 357, 288
- Myers P.C., Benson P.J. 1983, ApJ 266, 309
- Nejad L.A.M., Wagenblast R. 1999, A&A 350, 204
- Nilsson A., Hjalmarson Å., Bergman P., Millar T.J. 2000, A&A *in press*
- Nummelin A., Bergman P., Hjalmarson Å., Friberg P., Irvine W.M. 2000, ApJ *in press*
- Poynter R.L., Pickett H.M. 1985, Appl. Opt. 24, 2335
- Prasad S.S., Huntress W.T., Jr. 1982, ApJ 260, 590
- Pratap P., Dickens J. E., Snell R. L., et al. 1997, ApJ 486, 862
- Prusti T., Clark F.O., Whittet D.C.B., Laurejs R.J., Zhang C.Y. 1991, MNRAS 251, 303
- Rawlings J.M.C., Hartquist T.W., Menten K.M., Williams D.A. 1992, MNRAS 255, 471
- Reipurth B., Nyman L.-Å., Chini R. 1996, A&A 314, 258
- Ruffle D.P., Hartquist T.W., Taylor S.D., Williams D.A. 1997, MNRAS 291, 235
- Ruffle D.P., Hartquist T.W., Caselli P., Williams D.A. 1999, MNRAS 306, 691
- Sastry K.V.N.L., Lees R.M., Van der linde J. 1981, J. Mol. Spec 88, 228
- Spitzer, L. Jr. 1978, *Physical Processes in the Interstellar Medium*, John Wiley & Sons, New York, Ch. 13.3
- Suzuki H., Yamamoto S., Ohishi M., et al. 1992, ApJ 392, 551
- Swade D.A. 1989, ApJ 345, 828
- Talbi D., Herbst E. 1998, A&A 333, 1007
- Townes C.H., Schawlow A.L. 1975, *Microwave Spectroscopy*, Dover Publications Inc., New York
- Turner B.E., Lee H.-H., Herbst E. 1998, ApJS 115, 91
- Turner B.E., Terziewa R., Herbst E. 1999, ApJ 518, 699
- van Dishoeck E.F., Blake G.A. 1998, ARA&A 36, 317
- Vanhala H.A.T., Cameron A.G.W. 1997, ApJ 508, 291
- Vrtilek J.M., Gottlieb C.A., Thaddeus P. 1987, ApJ 314, 716
- Yamamoto S., Saito S., Kawaguchi K., et al. 1990, ApJ 361, 318